A cooperative DNA catalyst

Dallas N. Taylor[1,3†], Samuel R. Davidson[2†] and Lulu Qian[1,2,3⋆]
[1] *Computation and Neural Systems,* [2] *Bioengineering, and* [3] *Computer Science*
California Institute of Technology, Pasadena, CA 91125, USA
[†] *Equal contribution,* [⋆] *e-mail: luluqian@caltech.edu*

Supporting information

S1 Materials and methods

S1.1 Sequence design

DNA sequences of the cooperative catalytic circuit were designed following the principles outlined in Supplementary Note S1.1 of the previous work on seesaw DNA circuits[1] and are listed here in Table S1.

To ensure that all double-stranded domains are stably bound in all initial, intermediate, and final species, we chose the length of domains S1, S2, and S3 to be 10 nucleotides: when T1, T2, T3, and T4 are 5 nucleotides or longer, the shortest double-stranded domains in the intermediate species will be at least 15 nucleotides. For example, these double-stranded domains include T3+S2 when the input is fully bound to the gate (XGY), S1+T3 when the activator is fully bound to the gate (GYA), and S3+T4 when the fuel is fully bound to the translator (FGZ).

Sequences of S1, S2, and S3 were drawn from a pool of 10-nt domains generated by the software developed for seesaw DNA circuits,[1] and sequences of T1, T2, and T3 were drawn from a list of experimentally verified 7-nt toeholds designed for a DNA strand-displacement oscillator.[2] In cases when T3 was shortened from 7 to 5 or 4 nucleotides, the desired number of nucleotides were simply removed from the 3' end of the toehold sequence in the gate and fuel species while the translator was kept unchanged. Sequences of T4 and S4 were predetermined for compatibility with an existing reporter.[3,4]

To reduce spurious interactions between T2$*$ and S3 on the gate and promote availability of the open toehold, T2 was selected to contain A and T only while S3 was selected to contain T and C only. To reduce 0-toehold leak reaction between the gate and fuel, S1 and S2 were selected to contain a C at their 3' and 5' ends, respectively – compared to A-T base pair, C-G base pair causes less breathing at the end of a double helix.

When investigating the catalytic behavior of the activator, we used wobbles and mismatches to bias branch migration and favor the release of the activator for completing a catalytic cycle. Specifically, a wobble was introduced to the 8th nucleotide and mismatches to the 7th and 8th nucleotides on the 5' end of the S2 domain in the activator but not in the fuel. The same wobble and mismatches were also employed in the output initially bound to the gate (named output/gate-t in Table S1, where gate-t indicates gate top strand) so that branch migration in output production remains unbiased. Wobble or mismatch positions closer to the 5' end of S2 were not explored because they would reduce the stability of the double-stranded domain and encourage undesired leak reaction between the gate and fuel.

Similar to the clamp design in seesaw DNA circuits,[1] a 2-nt clamp domain was embedded in the translator and reporter for inhibiting leak reaction between the two that could be initiated by a stacking bond between the ends of the two helices. Since the clamp domain is not present in the output strand, the translation reaction is effectively reversible, while the forward reaction should be at least 100 times faster than the backward reaction because of the length difference between the initiation and dissociation toeholds.

NUPACK[5] analysis was performed for all designed species to verify their equilibrium concentrations and minimum free energy (MFE) structures at 25 °C with 100 nM of each strand. In particular, we confirmed that intermediate species XGY and GYA should be sufficiently stable even when T3 is 4 nucleotides, and the gate should be sufficiently stable with wobbles and mismatches at the chosen positions.

S1.2 Sample preparation

DNA oligonucleotide synthesis. All strands were chemically synthesized by Integrated DNA Technologies (IDT). Strands covalently bonded to a fluorophore or quencher were ordered HPLC-purified while unmodified strands were ordered with standard desalting only. Formulation service LabReady was selected so that all strands were delivered

at approximately 100 μM in IDTE, IDT's formulation of Tris-EDTA (TE) buffer (10 mM Tris, 0.1 mM EDTA, pH 8.0). On arrival, concentration of each strand was verified on a NanoDrop (Thermo Fisher) by averaging three measurements of absorbance at 260 nm for a 1 μL droplet. DNA was stored at 4 °C.

Annealing protocol and buffer condition. The two strands in the gate and translator were mixed in a 1:1 ratio and annealed at 45 μM. The reporter was annealed at 20 μM with the top quencher strand and bottom fluorophore strand in a 6:5 ratio – the concentration of the reporter was determined by the concentration of the bottom strand; excess top strand was used here because it should not react with any other molecules in the circuit and it helps ensure that all copies of the fluorophore strand should be bound to a quencher strand. The buffer for all double-stranded complexes was TE with 12.5 mM Mg^{2+}. To anneal, the following protocol was run on a thermal cycler (Eppendorf): hold at 90 °C for 2 minutes, ramp down to 20 °C by 1 °C per 60 seconds.

Purification. Following annealing, polyacrylamide gel electrophoresis (PAGE) was used to purify gate and translator on a 12% gel. A single desired band for each complex was cut, diced, and incubated for at least 24 hours at room temperature (approximately 24 °C) in TE buffer with 12.5 mM Mg^{2+}, during which period DNA should diffuse out of the gel and into the buffer. Gel fragments were then discarded. Concentrations of purified complexes were measured on a NanoDrop (Thermo Fisher).

S1.3 Fluorescence kinetics experiments

In each set of experiments, 110 μL of each sample was mixed at a standard concentration (1×) of 100 nM in a 96-well plate (Corning). Fluorescence levels were read every 2 minutes using a microplate reader (Cytation 5, Biotek) at 25°C. Excitation and emission wavelengths were set to 598 and 629 nm, respectively, for fluorophore ATTO590.

To reduce the loss of DNA to the surfaces of pipette tips and tubes, 2 μM of a 20-nt poly-T strand[6] (referred to as 20T below) was added first to each sample, and LoRetention tips and DNA LoBind tubes (Eppendorf) were used in all experiments.

In each set of fluorescence kinetics experiments with varying input and activator concentrations, a master mix was made with 20× 20T, 1× gate, 2× fuel, 1.5× translator, and 1.5× reporter. The master mix was transferred to a number of wells on a plate, and distinct amounts of input and activator were then added to each of the wells – compared to preparing each sample separately, the master mix allows for improved consistency across experiments.

S1.4 Data normalization

Each set of fluorescence kinetics experiments included a negative control with 0× input and 0× activator as well as a positive control with 1× input and 1× activator. The minimum raw fluorescence was determined by the averaging the initial five measurements of the negative control, and the maximum raw fluorescence was determined by averaging the final five measurements of the positive control. The minimum and maximum raw fluorescence were then used as 0× and 1×, respectively, to convert fluorescence data to concentration data. In this data normalization method, 0 nM (0×) is interpreted as the background fluorescence of the reaction mixture before any signal has been detected, and 100 nM (1×) is interpreted as the highest fluorescence of the reaction mixture after the output strand Y has been fully released from the gate, translated to signal Z, and detected by the reporter.

S2 Concept of three types of catalysts

In theory, DNA strand-displacement (DSD) systems are capable of implementing arbitrary chemical kinetics,[7] including any desired type of catalyst. The underlying principle is that for any given chemical reaction that involves a set of signal species (e.g. X and Y shown in Figure S1), auxiliary species (e.g. GY and F) can be designed to facilitate the desired interactions between signals. To achieve systematic implementation of chemical reaction networks (CRNs) where each signal species can participate in multiple distinct reactions, two criteria are necessary. First, there should be no sequence dependence across signals. For example, if the sequence of Y depends on the sequence of X, then $X1 \rightarrow X1 + Y$ and $X2 \rightarrow X2 + Y$ could result in a conflict where no sequence of Y satisfying both reactions exists. On the other hand, the sequences of auxiliary species do depend on the signal species – for example, GY designed to facilitate the production of Y when X is present must incorporate two domains of sequences that are determined by the sequences of X and Y, respectively. The sequence dependence between signal and auxiliary species does not affect the composability of individual reactions, because auxiliary species designed for one reaction should not participate in any other reactions and thus can be viewed as internal to each reaction. Second, all signals should have the same format (e.g. a toehold followed by a branch migration domain). If reactant X and product Y have different formats in $X \rightarrow X+Y$, then $Y \rightarrow Y+Z$ cannot use the same implementation scheme due to a conflict of Y having the format of a product in one reaction and that of a reactant in the other. Note that product species commonly contain history domains that do not participate in downstream reactions – in chemical reaction networks that consist of irreversible reactions (such as $X \rightarrow X + Y$), these history domains do not need to be considered for comparing the format of signal species.

Various CRN-to-DSD implementation schemes have been proposed,[7–9] yet successful experimental demonstrations have so far been limited to relatively simple systems involving up to three non-catalytic bimolecular reactions.[2,10] If behaviors as general as arbitrary chemical kinetics or Turing-universal computation are not required, DNA strand-displacement implementations of catalysts alone can be scalable. Systems with dozens of catalytic reactions in the form of $X \rightarrow X+Y$ have been demonstrated for performing digital logic and neural network computation.[1,4] Previous work has shown that the scalability of DNA strand-displacement systems depends on the simplicity of the motifs – when only one and two-stranded molecules were involved in synthesizing a system (at its initial state before any input signal arrives), the system behavior was robust to oligonucleotide synthesis errors and potential malformation of annealed structures.[3] Thus we are motivated to understand whether catalysts with enhanced functionality can be implemented with simple DNA strand-displacement motifs where each initial molecule consists of no more than two strands.[11]

First, $X \rightarrow X+Y$ can be extended with allosteric control $X+A \rightarrow X+Y$, where output Y is only produced when a consumable activator A is present. DNA strand-displacement implementation for this type of catalyst has been developed using two auxiliary species including a two-stranded gate and a single-stranded fuel (named GY and F in Figure S1).[12] In that implementation, the activator strand is consumed in forming a two-stranded product AY, which is functionally equivalent to Y because the activator strand only covers up a portion of the output strand not involved in downstream reactions. The input X and activator A have sequence dependence (a toehold complementary to each other) and different formats (a toehold followed by a branch migration domain vs. two concatenated toeholds), both of which pose some challenges for the implementation to be used in larger systems.

Next, $X \rightarrow X + Y$ can be extended from unimolecular to bimolecular $X + A \rightarrow X + A + Y$, where in addition to catalyst X, a second catalyst A is required for the production of Y. This second catalyst can be viewed as an activator that provides allosteric control for $X \rightarrow X + Y$ without being consumed itself. More generally, both X and A are signal species that cooperatively and catalytically produce Y. In this work, we develop a DNA strand-displacement implementation for the cooperative catalyst. As simple as the previous examples of basic DNA catalyst and allosteric DNA catalyst discussed above, the cooperative DNA catalyst also uses two auxiliary species including a two-stranded gate and a single-stranded fuel. Unlike the allosteric DNA catalyst discussed above and other more complex variations previously developed,[13,14] the cooperative DNA catalyst that we show here requires no sequence dependence between two input signals X and A. With a simple, two-stranded translator, output Y can be converted to the same format as either input with independent sequence (Figures S5b and S5c).

The difference in the abstract chemical reactions of the three types of catalyst determines their distinct usages in various scenarios. For example, when auxiliary species are in large excess, their concentrations can be treated as roughly constant. In this scenario, a constant rate of output production can be controlled by the concentration(s) of the catalyst(s). For the allosteric catalyst with a consumable activator, the system behavior is similar to the basic catalyst if the activator is in large excess, otherwise the rate of output production will decrease as the activator

is used up. For the cooperative catalyst, the rate of output production scales linearly with both catalysts, which could be used for computing the multiplication of two real numbers when combined with a degradation reaction.[15] Alternatively, in a second scenario, the concentrations of auxiliary species can be used to control the completion level of output production, while the presence or absence of the catalyst(s) are used to turn ON or OFF output production. The concentration of a consumable activator in the allosteric catalyst can also be used to determine output completion, so long as it is less than the concentrations of auxiliary species – this behavior is useful for learning an analog weight in chemical neural networks.[16] By contrast, with the cooperative catalyst, the output completion solely depends on the concentrations of auxiliary species – this behavior is useful for learning a binary weight in chemical neural networks.[17] While the simulations of these two scenarios shown in Figure S1 provide a characteristic understanding for certain example behaviors, the exact kinetics for each type of catalyst is a tunable variable. As the rate of DNA strand-displacement reactions can be well controlled by the length and sequence of toeholds,[18,19] desired kinetics can be tailored for different usages of the catalysts by altering the toehold designs.

	Basic catalyst	Allosteric catalyst	Cooperative catalyst
Abstract chemical reaction	$X \rightarrow X + Y$	$X + A \rightarrow X + Y$	$X + A \rightarrow X + A + Y$
DNA strand-displacement implementation	$X + GY \rightleftharpoons XG + Y$ $XG + F \rightleftharpoons X + GF$	$A + GY \rightleftharpoons AGY$ $X + AGY \rightleftharpoons XG + AY$ $XG + F \rightleftharpoons X + GF$	$X + A + GY \rightleftharpoons XGA + Y$ $XGA + F \rightleftharpoons X + A + GF$
Simplified overall reaction	$X + GY + F \xrightarrow{k} X + Y$	$X + A + GY + F \xrightarrow{k} X + Y$	$X + A + GY + F \xrightarrow{k} X + A + Y$
Steady-state output concentration	$[Y]_\infty = \min([GY]_0, [F]_0)$ if $[X]_0 > 0$	$[Y]_\infty = \min([A]_0, [GY]_0, [F]_0)$ if $[X]_0 > 0$	$[Y]_\infty = \min([GY]_0, [F]_0)$ if $[X]_0, [A]_0 > 0$
Example scenario 1 with controlled constant rate of output production	$[GY]_t, [F]_t \approx$ constant $[Y]_t = \alpha [X]_0 \cdot t$ 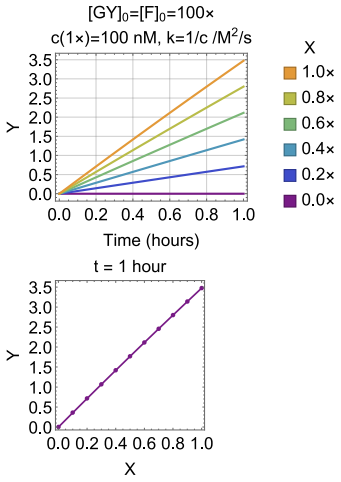	$[A]_t, [GY]_t, [F]_t \approx$ constant $[Y]_t = \alpha [X]_0 \cdot t$ 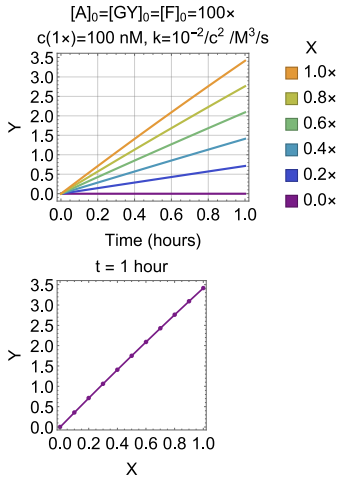	$[GY]_t, [F]_t \approx$ constant $[Y]_t = \alpha [X]_0 [A]_0 \cdot t$ 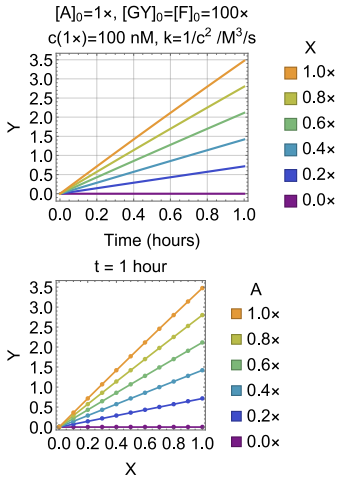
Example scenario 2 with controlled completion level of output production	$[F]_0 \geq [GY]_0$ $[Y]_\infty = [GY]_0$ if $[X]_0 > 0$ 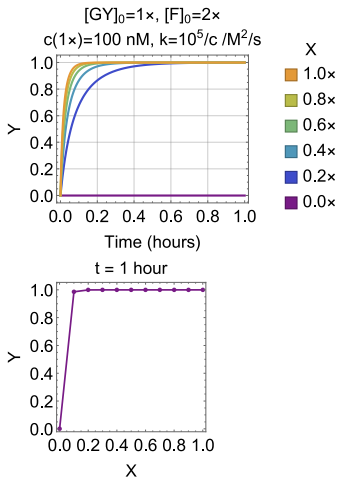	$[F]_0 \geq [GY]_0 \geq [A]_0$ $[Y]_\infty = [A]_0$ if $[X]_0 > 0$ 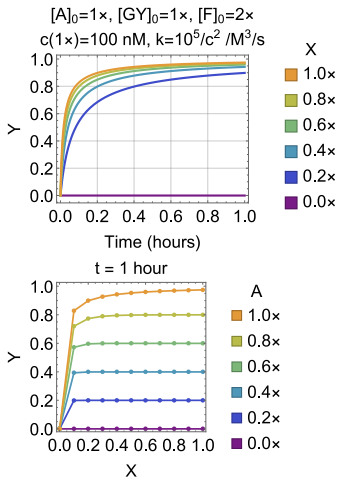	$[F]_0 \geq [GY]_0$ $[Y]_\infty = [GY]_0$ if $[X]_0, [A]_0 > 0$ 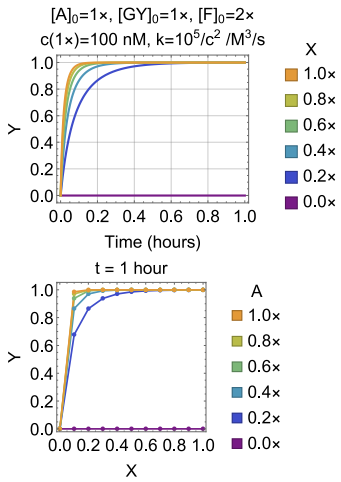

Figure S1: **Concept of three types of catalysts.** In DNA strand-displacement implementations, signal species are colored in black, auxiliary species are colored in gray, and intermediate and waste products are colored in blue. Characteristic simulations for example scenarios were performed using the simplified overall reaction.

S3 Modeling and simulation of cooperative catalyst

All simulations were performed with mass-action kinetics using CRNSimulator.[20]

The following reactions were used to model reversible cooperative hybridization $X + A + GY \rightleftharpoons XGA + Y$, where k_b'' was introduced for understanding the effect of wobble and mismatch:

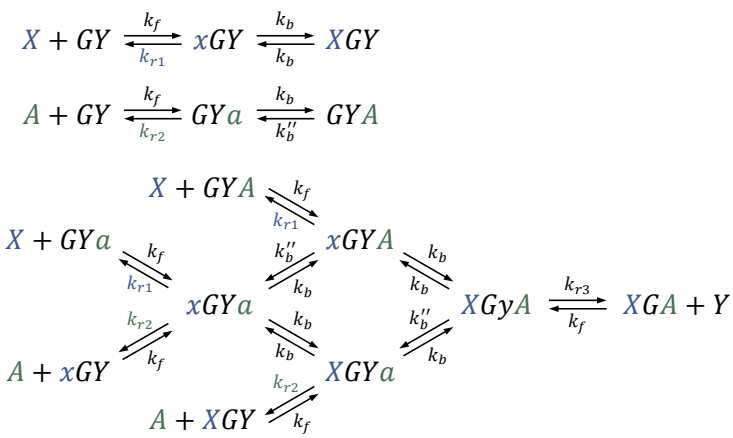

$X + A + GF \rightleftharpoons XGA + F$ was modeled similarly, where k_b' was introduced for understanding the effect of wobble and mismatch:

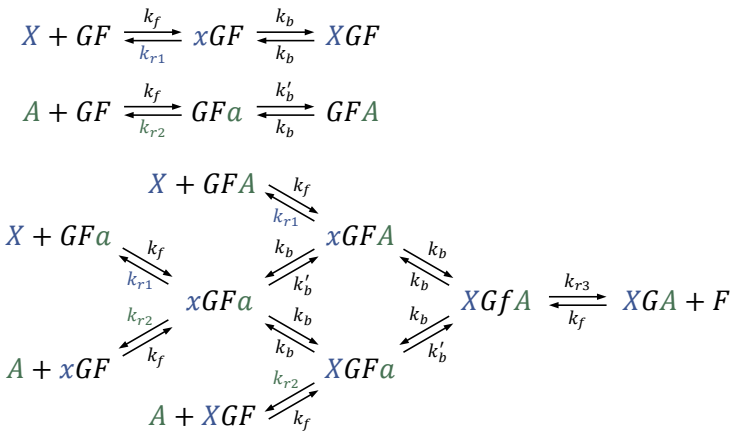

Output Y reacting with translator GZ was modeled as follows, where k_{r3}' is dissociation rate of T3 binding to the translator and k_{rc} is dissociation rate of a 2-nt clamp:

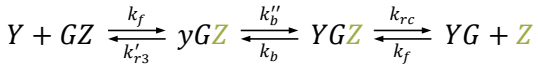

Fuel F can also react with translator GZ but the reaction is reversible without producing signal Z:

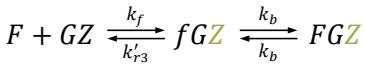

Signal Z reacting with reporter R was modeled as follows, where k_s is effective rate of an irreversible strand displacement reaction with a 5-nt toehold:

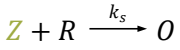

The following rate constants were used in all simulations:

$$
\begin{aligned}
k_f &= 2 \times 10^6 \text{ /M/s} \\
k_{r1} &= 0.1 \text{ /s} \\
k_{r2} &= 0.2 \text{ /s} \\
k_{r3} &= 0.001 \text{ /s, } 0.015 \text{ /s, and } 0.03 \text{ /s for T3 = 7, 5, and 4 nucleotides, respectively.} \\
k'_{r3} &= 0.33 \text{ /s, } 5 \text{ /s, and } 10 \text{ /s for T3 = 7, 5, and 4 nucleotides, respectively.} \\
k_b &= 1 \text{ /s} \\
k'_b &= 1 \text{ /s and } 0.2 \text{ /s for S2 domain without and with a wobble, respectively.} \\
k''_b &= 1 \text{ /s and } 0.02 \text{ /s for S2 domain without and with a wobble, respectively.} \\
k_{rc} &= 10^4 \text{ /s} \\
k_s &= 10^5 \text{ /M/s}
\end{aligned}
$$

k_{r1} (the dissociation rate of toehold T1) is smaller than k_{r2} (the dissociation rate of toehold T2), because the observed kinetics with 1× input and 0.1× activator (Figure 5b) was slightly slower than that with 0.1× input and 1× activator (Figure 4d). Presumably, this could be due to the sequence difference in toeholds T1 and T2 or the structural asymmetry of the gate:output molecule – the single-stranded S3 and T4 domains could partially inhibit the open toehold T2$*$ through spurious binding.

Understanding the biophysics and kinetics of reversible cooperative hybridization merits future study. The model in this work does not fully explain the behavior of the system. For example, a 30-fold difference in dissociation rate k_{r3} was estimated comparing a 7-nt and 4-nt toehold, which is significantly less than the 1000-fold difference suggested in previous studies.[18,19] Moreover, taking the additional stacking bond into consideration as roughly 1-nt energy, the 4-nt toehold dissociation rate (0.03 /s) is still much smaller than expected (10 /s). A more detailed model at the base-pair level would be particularly useful for a better understanding of the effect of a wobble.[21]

S4 Sequence-level design diagrams

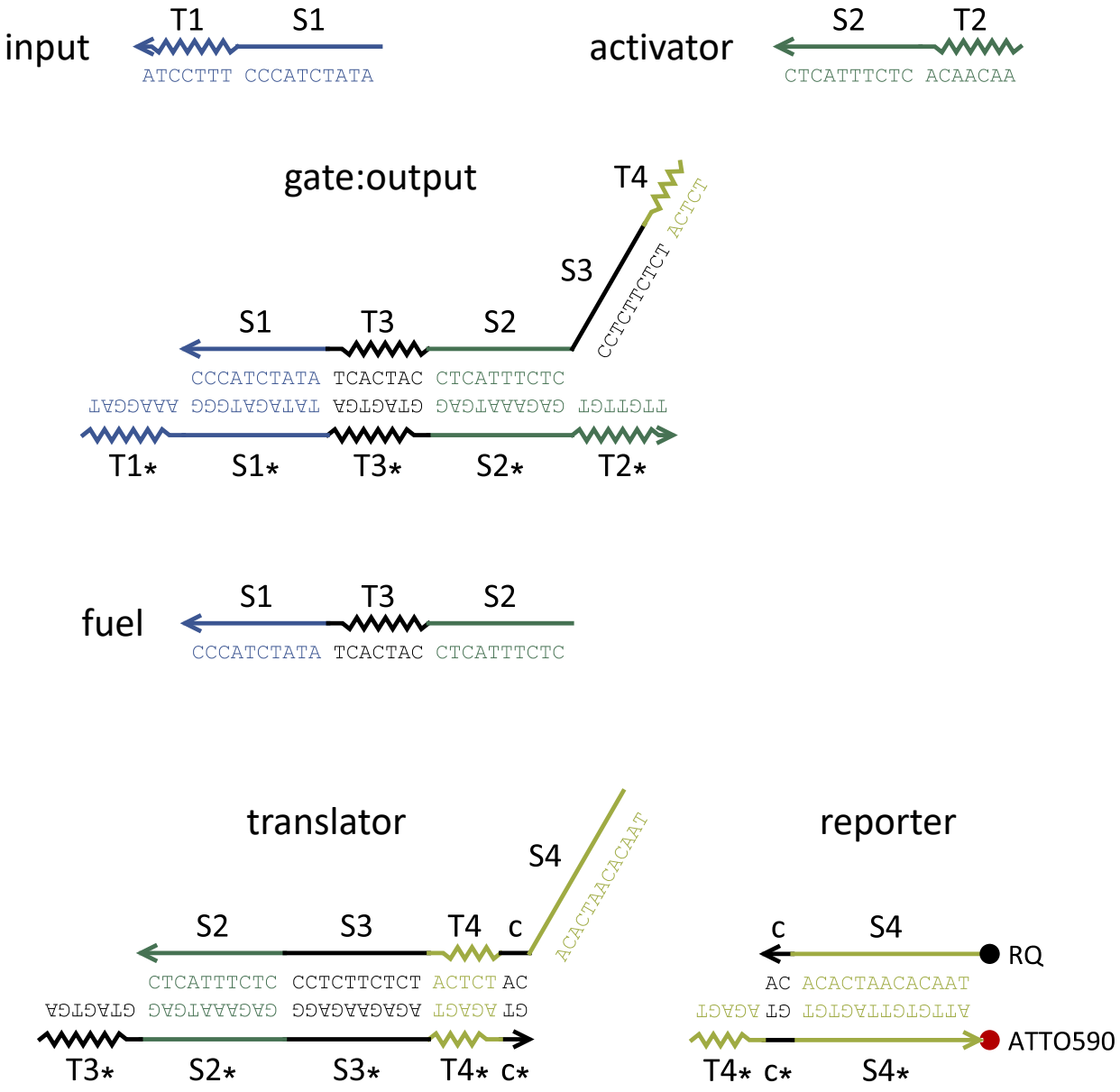

Figure S2: **Sequence-level diagrams.** A 2-nt clamp domain is labeled as c. A 7-nt toehold T3 and branch migration domain S2 without any wobbles or mismatches are shown here. Sequences for varying lengths of toehold T3 and branch migration domain S2 with a wobble or mismatch are listed in Table S1.

S5 Effect of a wobble or mismatch for promoting activator recycling

Previous studies have shown that a mismatch (i.e. non-Watson–Crick base pairs) in the branch migration domain of the invader strand has an effect of slowing down strand displacement, the kinetics of which depends on the position and nucleotide sequence of the mismatch for a given toehold.[21–23] This effect is useful for improving the performance of DNA catalysts. For example, leak between a gate complex and a fuel strand can be reduced by introducing mismatch modifications in the fuel strand.[24] Desired output production can be sped up by the introduction of mismatch modifications in the input and output strands, which favors the process of fuel releasing the input.[25]

Here we investigate whether the above principle of mismatches can be applied to improve the performance of the cooperative catalyst. Specifically, we aim to use a G·T wobble,[26] which is known to be more stable than other types of mismatches,[27] to promote activator recycling without increasing leak.

Unlike the experiments shown in Figure 5c, unpurified gate:output and translator complexes were used in the following experiments that we initially performed for evaluating the effect of wobbles compared with mismatches. Without gel purification, it is possible that the double-stranded complexes contained excess single strands due to stoichiometry errors or otherwise contained a small fraction of malformed structures. This impurity led to a type of behavior similar to thresholding, where the output production appeared much slower compared to experiments with purified complexes, as if the activator was at a much lower concentration than expected. For example, $0.001\times$ activator was used in simulations (Figure S3d) in order to roughly agree with the experiments with $0.1\times$ activator (Figure S3c). Thus, the impurity allowed us to evaluate the robustness of the activator promoted by a wobble.

We introduced a wobble modification (i.e. changing a C to a T) at varying positions within the S2 domain in the activator and output strands, while keeping the fuel perfectly complementary to the gate strand (Figure S3a). When the activator but not the output strand was modified, the output production became slower (Figure S3b), indicating that the biased branch migration in output release played a more significant role than the biased branch migration in activator recycling (i.e. activator release by fuel). However, when the activator and output strands were both modified, the output production became faster, especially for wobble modification at position 8 (Figure S3b). In this case, only two out of the four possible positions were explored experimentally because more fraying is expected in the gate:output complex for modification at positions 1 and 3 in the output strand, which will likely result in increased leak between the complex and fuel.

We then compared the wobble modification at position 8 with a mismatch modification at the same and an adjacent position (Figure S3c). Interestingly, the output production was faster with the wobble than the mismatches (Figure S3c, left plot), while the leak was slower (Figure S3c, right plot).

To better understand the observed system behavior, we used simulations to estimate the bias in branch migration rates affected by the wobble at position 8 (Figure S4). We found that a bias in branch migration involving the activator and fuel alone cannot explain the faster output production in experiments (Figure S4a). It is necessary that a bias also exists in branch migration involving the activator and output (Figure S4b). This bias is reasonable because position 8 is near the end of branch migration for the activator and near the beginning of branch migration for the output, while branch migration is expected to slow down more significantly for non-Watson-Crick base pairs near the beginning.[21,23] Because the bias in branch migration involving the activator and fuel still has some effect on the overall rate of output production, it is desirable that the wobble is not too close to the end of branch migration for the activator (e.g. position 10). Moreover, simulations suggested that a bias in branch migration involving the input and output, together with the above biases, could further speed up output production (Figure S4c) – this would be useful for future developments such as an activator-producing threshold discussed in Supplementary Note S7.

While a wobble in branch migration domain S2 resulted in faster kinetics when the activator concentration was low (Figure S3c), it resulted in slower overall kinetics when the activator concentration was relatively high (Figure 5c). This is because the branch migration rate of the output reacting with the translator also slowed down with the wobble (Supplementary Note S3). This slowdown in the translation reaction explains why too much increase in k_b/k_b'' decreases the overall signal production in simulations (Figure S4). If needed, the translator can be redesigned with S2′ and S2′∗ domain sequences in the top and bottom strands, respectively, to match the modified domain sequence S2′ in the output strand.

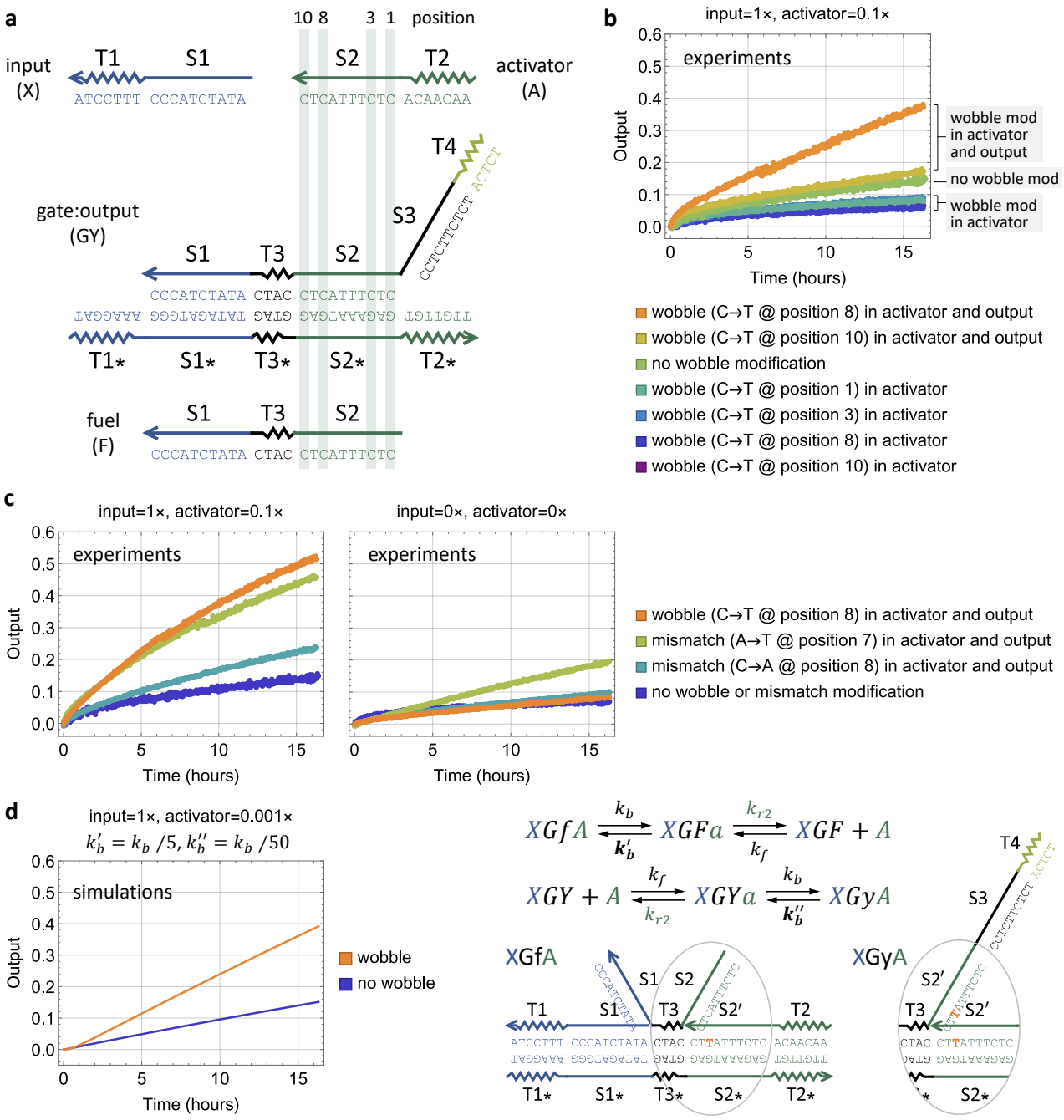

Figure S3: **Robustness of the activator with unpurified gates.** **(a)** Sequence-level diagrams with labeled nucleotide positions in the S2 domain. **(b, c)** Fluorescence kinetics data for the cooperative catalyst without or with a (b) wobble or (c) mismatch modification in the activator and output strands. **(d)** Simulations without or with modified branch migration rate constants attributed to a wobble. Standard concentration $1\times = 100$ nM. Initial concentrations of gate:output, fuel, translator, and reporter are $1\times$, $2\times$, $1.5\times$, and $1.5\times$, respectively. Output is shown as a relative concentration to $1\times$. The experiment for wobble modification at position 8 in activator and output shown in b and c are two repeats of the same experiment performed on different days; the difference in kinetics is likely due to experimental noise.

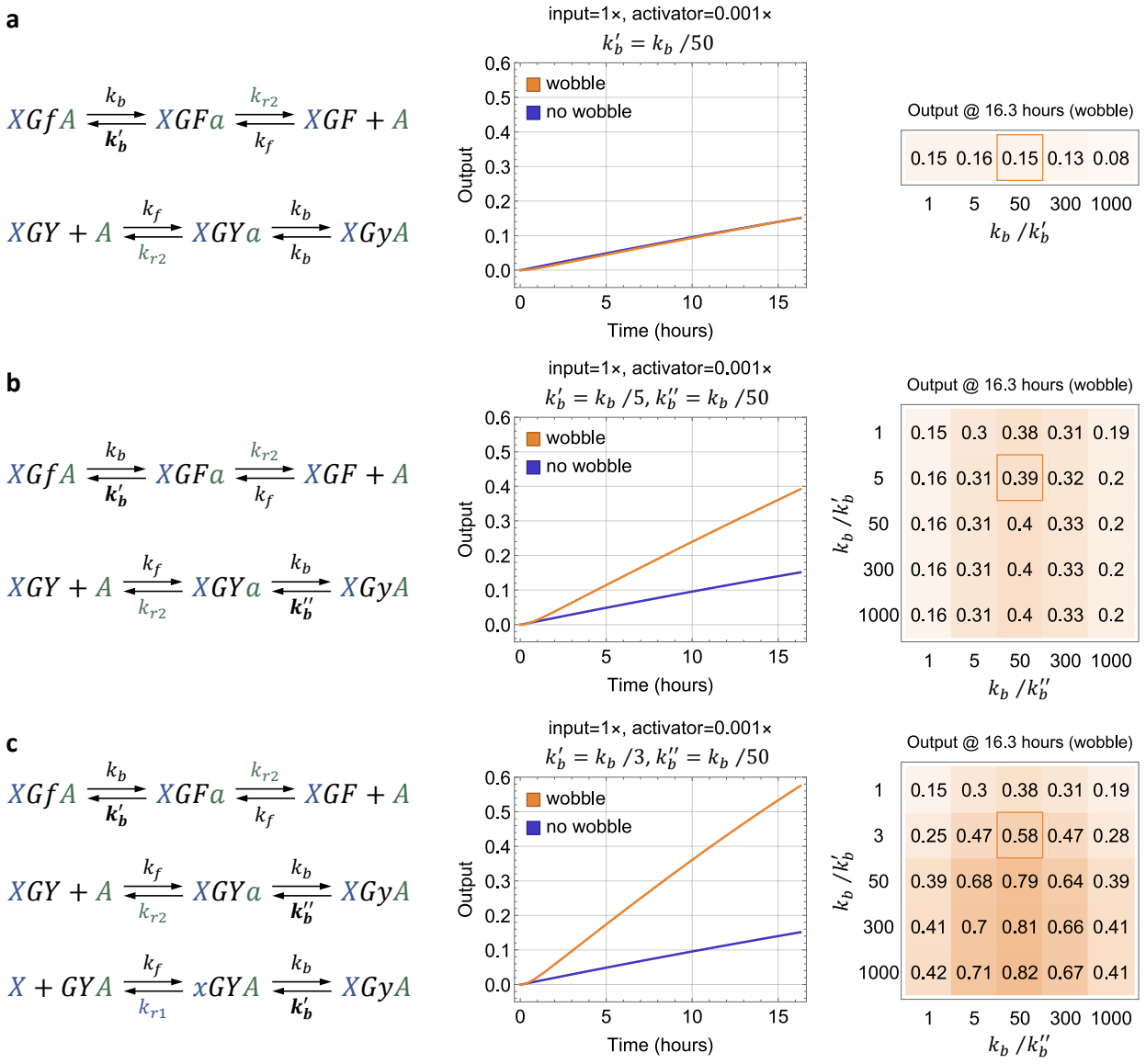

Figure S4: **Simulation analysis of the effect of wobble.** **(a)** Simulations with a bias in branch migration involving the activator and fuel (first reaction, k_b: fuel displacing activator, k'_b: activator displacing fuel, $k_b \geq k'_b$). **(b)** Simulations with the above bias and a bias in branch migration involving the activator and output (second reaction, k_b: activator displacing output, k''_b: output displacing activator, $k_b \geq k''_b$). **(c)** Simulations with the above biases and a bias in branch migration involving the input and output (third reaction, k_b: input displacing output, k'_b: output displacing input, $k_b \geq k'_b$). Representative reactions are shown here, and the full list of reactions involving the modified branch migration rates are shown in Supplementary Note S3. Standard concentration $1\times = 100$ nM. Initial concentrations of gate:output, fuel, translator, and reporter are $1\times$, $2\times$, $1.5\times$, and $1.5\times$, respectively. Output is shown as a relative concentration to $1\times$. Kinetics trajectories for one example ratio of branch migration rates are shown in the plot, while the relative concentration of the output at 16.3 hours (time of the last data point in the kinetics plot) is shown in an array with varying ratios of branch migration rates. The orange box in the array highlights the example shown in the kinetics plot.

S6 An AND gate with near-perfect signal restoration

The cooperative catalyst could be used to build a better AND gate. It is important to embed signal restoration within DNA circuits for cleaning up noise and resolving signal decay. An implementation of DNA logic gates has been proposed with the aim of processing input signals with substantial noise (OFF $= 0-0.4\times$ and ON $= 0.6-1\times$),[28] but the complexity of the design has inhibited successful experimental demonstration (a two-input AND gate requires 5 gates, 5 thresholds, and 2 fuel strands). With the cooperative catalyst, the desired logic function could be implemented with a much simpler design (1 gate, 2 thresholds, and 1 fuel strand as shown in Figure S5a). Because the two input strands in the cooperative catalyst have independent domain sequences, two distinct threshold complexes can be designed without any concern of threshold crosstalk.[1]

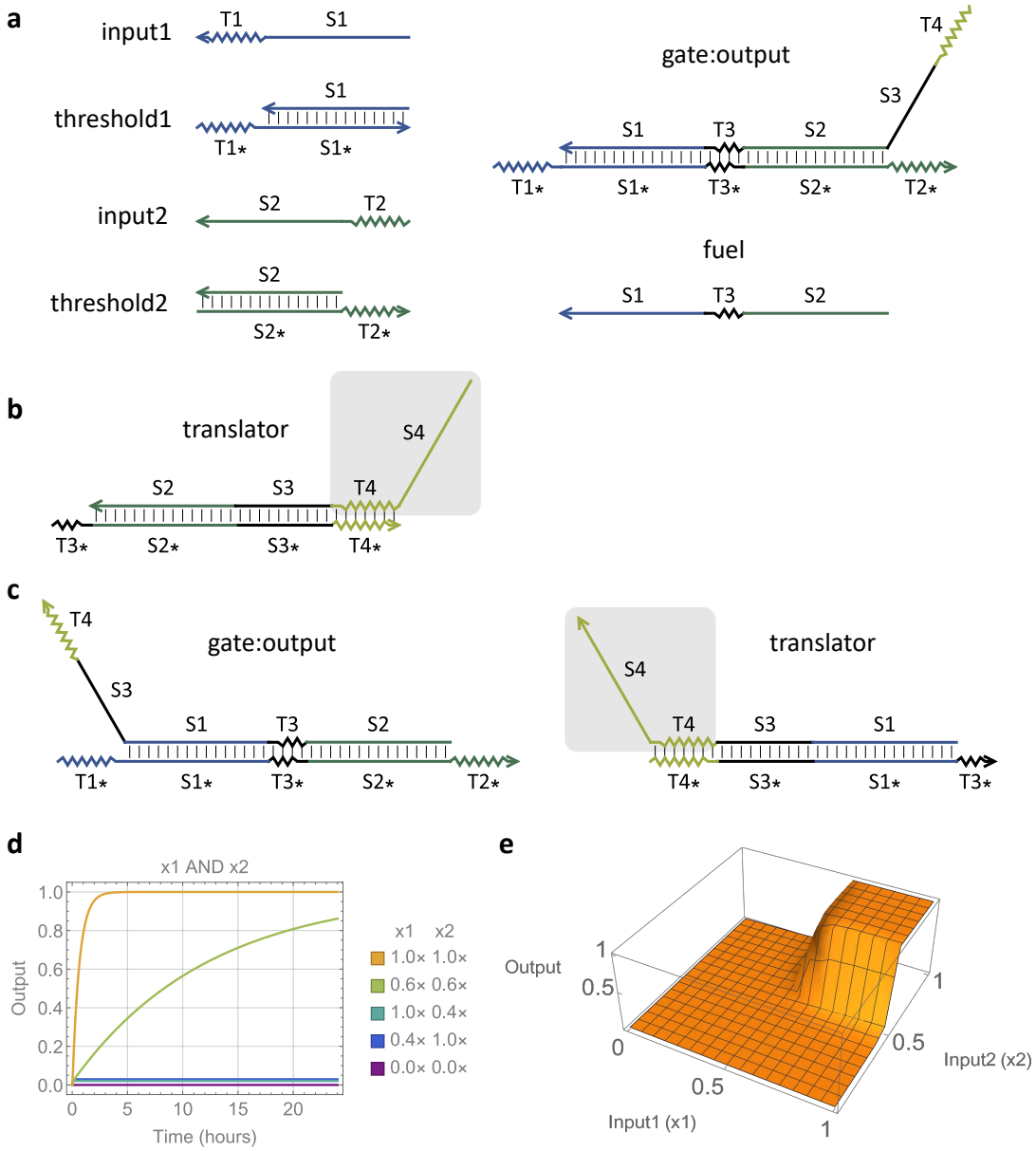

Figure S5: **An AND gate with near-perfect signal restoration. (a, b)** Design diagrams of (a) an AND gate and (b) a translator producing a signal strand that has the same format as input1. **(c)** An alternative gate and translator design for producing a signal with the same format as input2. One of the two designs can be used for each AND gate in a logic circuit, depending on which input format its downstream gate requires. **(d)** Simulated kinetics of the AND gate with five example input combinations. **(e)** Simulated input-output relationship at $t = 24$ hours. Standard concentration $1\times = 100$ nM.

S7 An activator-producing threshold

The cooperative catalyst could be used to develop a better threshold mechanism that combines the advantages of sequential[29] and competitive[1] thresholding. In sequential thresholding ($X + Th \rightarrow GY$ and $X + GY + F \rightarrow Y$), the threshold (Th) concentration must be the same as the gate (GY) concentration, which introduces an undesired constraint on how much noise can be suppressed in the input signal versus how much output signal can be produced. In competitive thresholding ($X + Th \xrightarrow{k_f} \emptyset$ and $X + GY + F \xrightarrow{k_s} X + Y$, $k_f \gg k_s$), there are no constraints between the threshold and gate concentrations, but the thresholding reaction must be much faster than the catalyst. With the cooperative catalyst, thresholding and signal amplification can be implemented in two sequential steps: $X + Th \rightarrow A$ and $X + A + GY + F \rightarrow X + A + Y$. This implementation (Figure S6a) neither requires a significant rate difference nor does there exist any dependence between threshold and output concentrations. The kinetics of the cooperative catalyst simulated here (Figure S6c) is not as fast as it could be. With further tuning of toehold sequences, possibly introducing wobbles or mismatches in both S1 and S2 domains, and using a faster translator, much faster signal restoration could potentially be achieved.

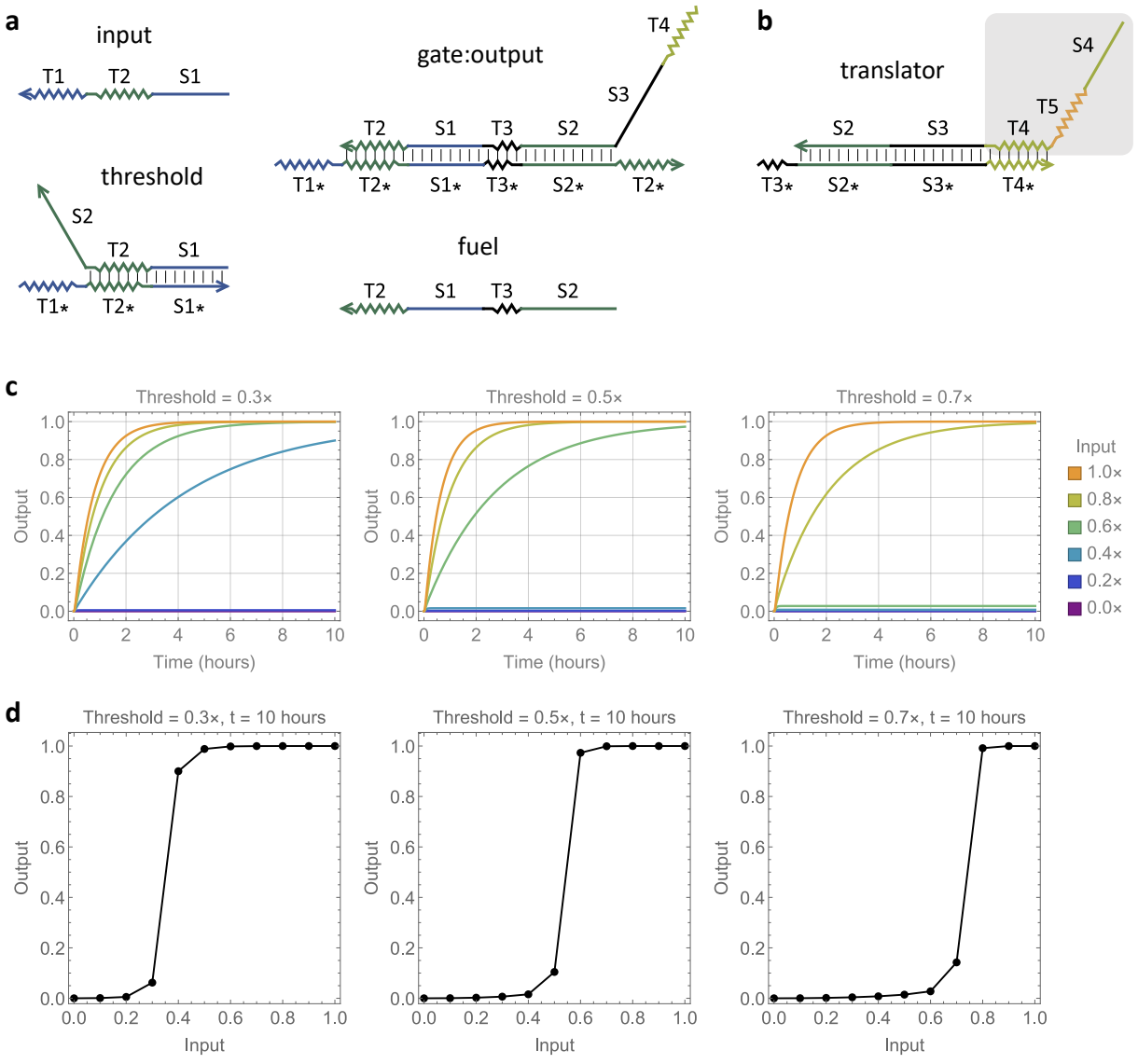

Figure S6: **An activator-producing threshold. (a, b)** Design diagrams of (a) a signal restoration circuit using an activator-producing threshold, and (b) a translator producing a signal strand that has the same format as the input. **(c)** Simulated kinetics of the signal restoration circuit with three example threshold and six example input values. **(d)** Simulated input-output relationship at $t = 10$ hours. Standard concentration $1\times = 100$ nM.

S8 DNA sequences

Table S1: DNA sequences of the cooperative catalyst. All sequences are listed from 5' to 3'.

Name	Sequence
output/gate-t (7ntT3)	TCTCA TCTCTTCTCC CTCTTTACTC CATCACT ATATCTACCC
output/gate-t (5ntT3)	TCTCA TCTCTTCTCC CTCTTTACTC CATCA ATATCTACCC
output/gate-t (4ntT3)	TCTCA TCTCTTCTCC CTCTTTACTC CATC ATATCTACCC
output/gate-t (4ntT3 and wobble10)	TCTCA TCTCTTCTCC CTCTTTACTT CATC ATATCTACCC
output/gate-t (4ntT3 and wobble8)	TCTCA TCTCTTCTCC CTCTTTATTC CATC ATATCTACCC
output/gate-t (4ntT3 and mismatch8)	TCTCA TCTCTTCTCC CTCTTTAATC CATC ATATCTACCC
output/gate-t (4ntT3 and mismatch7)	TCTCA TCTCTTCTCC CTCTTTTCTC CATC ATATCTACCC
gate-b (7ntT3)	TAGGAAA GGGTAGATAT AGTGATG GAGTAAAGAG TGTTGTT
gate-b (5ntT3)	TAGGAAA GGGTAGATAT TGATG GAGTAAAGAG TGTTGTT
gate-b (4ntT3)	TAGGAAA GGGTAGATAT GATG GAGTAAAGAG TGTTGTT
input	ATATCTACCC TTTCCTA
activator	AACAACA CTCTTTACTC
activator (wobble10)	AACAACA CTCTTTACTT
activator (wobble8)	AACAACA CTCTTTATTC
activator (wobble3)	AACAACA CTTTTTACTC
activator (wobble1)	AACAACA TTCTTTACTC
activator (mismatch8)	AACAACA CTCTTTAATC
activator (mismatch7)	AACAACA CTCTTTTCTC
fuel (7ntT3)	CTCTTTACTC CATCACT ATATCTACCC
fuel (5ntT3)	CTCTTTACTC CATCA ATATCTACCC
fuel (4ntT3)	CTCTTTACTC CATC ATATCTACCC
signal/translator-t	CATAACACAATCACA TCTCA TCTCTTCTCC CTCTTTACTC
translator-b	AGTGATG GAGTAAAGAG GGAGAAGAGA TGAGA TG
reporter-t	/5IAbRQ/ CATAACACAATCACA
reporter-b	TG AGA TGTGATTGTGTTATG /3ATTO590N/

References

[1] Lulu Qian and Erik Winfree. Scaling up digital circuit computation with DNA strand displacement cascades. *Science*, 332(6034):1196–1201, 2011.

[2] Niranjan Srinivas, James Parkin, Georg Seelig, Erik Winfree, and David Soloveichik. Enzyme-free nucleic acid dynamical systems. *Science*, 358(6369), 2017.

[3] Anupama J Thubagere, Chris Thachuk, Joseph Berleant, Robert F Johnson, Diana A Ardelean, Kevin M Cherry, and Lulu Qian. Compiler-aided systematic construction of large-scale DNA strand displacement circuits using unpurified components. *Nature Communications*, 8(1):1–12, 2017.

[4] Kevin M Cherry and Lulu Qian. Scaling up molecular pattern recognition with DNA-based winner-take-all neural networks. *Nature*, 559(7714):370–376, 2018.

[5] Joseph N Zadeh, Conrad D Steenberg, Justin S Bois, Brian R Wolfe, Marshall B Pierce, Asif R Khan, Robert M Dirks, and Niles A Pierce. NUPACK: analysis and design of nucleic acid systems. *Journal of Computational Chemistry*, 32(1):170–173, 2011.

[6] David Yu Zhang, Andrew J Turberfield, Bernard Yurke, and Erik Winfree. Engineering entropy-driven reactions and networks catalyzed by DNA. *Science*, 318(5853):1121–1125, 2007.

[7] David Soloveichik, Georg Seelig, and Erik Winfree. DNA as a universal substrate for chemical kinetics. *Proceedings of the National Academy of Sciences*, 107(12):5393–5398, 2010.

[8] Lulu Qian, David Soloveichik, and Erik Winfree. Efficient turing-universal computation with DNA polymers. In *International Workshop on DNA-Based Computers*, pages 123–140. Springer, 2010.

[9] Luca Cardelli. Two-domain DNA strand displacement. *Mathematical Structures in Computer Science*, 23(2):247–271, 2013.

[10] Yuan-Jyue Chen, Neil Dalchau, Niranjan Srinivas, Andrew Phillips, Luca Cardelli, David Soloveichik, and Georg Seelig. Programmable chemical controllers made from DNA. *Nature Nanotechnology*, 8(10):755–762, 2013.

[11] Robert F Johnson and Lulu Qian. Simplifying chemical reaction network implementations with two-stranded DNA building blocks. In Cody Geary and Matthew J. Patitz, editors, *International Conference on DNA Computing and Molecular Programming*, volume 174 of *Leibniz International Proceedings in Informatics (LIPIcs)*, pages 2:1–2:14. Schloss Dagstuhl-Leibniz-Zentrum für Informatik, 2020.

[12] Xiaolong Yang, Yanan Tang, Sarah M Traynor, and Feng Li. Regulation of DNA strand displacement using an allosteric DNA toehold. *Journal of the American Chemical Society*, 138(42):14076–14082, 2016.

[13] David Yu Zhang and Erik Winfree. Dynamic allosteric control of noncovalent DNA catalysis reactions. *Journal of the American Chemical Society*, 130(42):13921–13926, 2008.

[14] Xi Chen. Expanding the rule set of DNA circuitry with associative toehold activation. *Journal of the American Chemical Society*, 134(1):263–271, 2012.

[15] Marko Vasić, David Soloveichik, and Sarfraz Khurshid. CRN++: Molecular programming language. *Natural Computing*, 19(2):391–407, 2020.

[16] Matthew R Lakin and Darko Stefanovic. Supervised learning in adaptive DNA strand displacement networks. *ACS Synthetic Biology*, 5(8):885–897, 2016.

[17] Marko Vasic, Cameron Chalk, Sarfraz Khurshid, and David Soloveichik. Deep molecular programming: a natural implementation of binary-weight ReLU neural networks. In *International Conference on Machine Learning*, pages 9701–9711. PMLR, 2020.

[18] David Yu Zhang and Erik Winfree. Control of DNA strand displacement kinetics using toehold exchange. *Journal of the American Chemical Society*, 131(47):17303–17314, 2009.

[19] Niranjan Srinivas, Thomas E Ouldridge, Petr Šulc, Joseph M Schaeffer, Bernard Yurke, Ard A Louis, Jonathan PK Doye, and Erik Winfree. On the biophysics and kinetics of toehold-mediated DNA strand displacement. *Nucleic Acids Research*, 41(22):10641–10658, 2013.

[20] David Soloveichik. CRNSimulator. `http://users.ece.utexas.edu/~soloveichik/crnsimulator.html`, 2009.

[21] Patrick Irmisch, Thomas E Ouldridge, and Ralf Seidel. Modeling DNA-strand displacement reactions in the presence of base-pair mismatches. *Journal of the American Chemical Society*, 142(26):11451–11463, 2020.

[22] David Yu Zhang and Erik Winfree. Robustness and modularity properties of a non-covalent DNA catalytic reaction. *Nucleic Acids Research*, 38(12):4182–4197, 2010.

[23] Robert RF Machinek, Thomas E Ouldridge, Natalie EC Haley, Jonathan Bath, and Andrew J Turberfield. Programmable energy landscapes for kinetic control of DNA strand displacement. *Nature Communications*, 5(1):1–9, 2014.

[24] Xiaoping Olson, Shohei Kotani, Jennifer E Padilla, Natalya Hallstrom, Sara Goltry, Jeunghoon Lee, Bernard Yurke, William L Hughes, and Elton Graugnard. Availability: A metric for nucleic acid strand displacement systems. *ACS Synthetic Biology*, 6(1):84–93, 2017.

[25] Natalie EC Haley, Thomas E Ouldridge, Ismael Mullor Ruiz, Alessandro Geraldini, Ard A Louis, Jonathan Bath, and Andrew J Turberfield. Design of hidden thermodynamic driving for non-equilibrium systems via mismatch elimination during DNA strand displacement. *Nature Communications*, 11(1):1–11, 2020.

[26] Hatim T Allawi and John SantaLucia. Thermodynamics and NMR of internal G·T mismatches in DNA. *Biochemistry*, 36(34):10581–10594, 1997.

[27] John SantaLucia Jr and Donald Hicks. The thermodynamics of DNA structural motifs. *Annual Review of Biophysics and Biomolecular Structure*, 33:415–440, 2004.

[28] Lulu Qian and Erik Winfree. A simple DNA gate motif for synthesizing large-scale circuits. *Journal of the Royal Society Interface*, 8(62):1281–1297, 2011.

[29] Georg Seelig, David Soloveichik, David Yu Zhang, and Erik Winfree. Enzyme-free nucleic acid logic circuits. *Science*, 314(5805):1585–1588, 2006.